The electrical dislocation resistivity and the deviation from Matthiessen's rule of deformed high-purity aluminium

2000 J. Phys.: Condens. Matter 12 10499

(http://iopscience.iop.org/0953-8984/12/50/311)

J. Phys.: Condens. Matter **12** (2000) 10499–10514. Printed in the UK PII: S0953-8984(00)15681-4

The electrical dislocation resistivity and the deviation from Matthiessen's rule of deformed high-purity aluminium

E Schafler and F Sachslehner

Institut für Materialphysik der Universität Wien, Strudlhofgasse 4, A-1090 Wien, Austria†

E-mail: fsachs@ap.univie.ac.at (F Sachslehner)

Received 17 July 2000, in final form 11 October 2000

Abstract. The experimental dislocation resistivity of rolled samples of 99.9999% pure aluminium was investigated in the temperature range from 4.2 K to 300 K. The minimum in the deviation from Matthiessen's rule (DMR) below 40 K and the step height of the DMR from 4.2 K to 300 K can be explained by anisotropic scattering in terms of a three-group or a two-group model. The physical relevance of the fitted anisotropy parameters for electron–dislocation (A_d) and electron–phonon scattering (A_p) can be better seen in the two-group model. The variation of A_d and A_p with dislocation density is similar to that for the noble metals, whereby A_p at low temperatures is much more anisotropic for aluminium. The change of A_p with increasing dislocation density for $T \leqslant 50$ K can be understood if anisotropic small-angle scattering at local phonon modes originating from the dislocations is taken into account. This anisotropy could arise, as the Burgers vectors of the dislocations are oriented mainly in [011] directions.

1. Introduction

Few researchers have investigated the temperature dependence of the deviation from Matthiessen's rule of deformed high-purity aluminium [1–3] and dilute aluminium alloys [1]. An obvious feature is the occurrence of a minimum in the DMR curves at temperatures between 10 K and 40 K [1]. The situation is complicated by the fact that in deformed high-purity aluminium a proportion of the dislocations produced are already annealed at room temperature [1, 4]. Dislocations are annihilated more rapidly if the applied deformation is larger [4, 5]. Barnard [2] tried to explain the results of Endo *et al* [1] by using a three-group model (3GM) which had been successful for the interpretation of the temperature dependence of the resistivity below 50 K [6] and the low-field Hall coefficient of pure aluminium [7]. However, within this model the anisotropy parameters obtained for electron–dislocation scattering were rather doubtful as they depended very strongly on the dislocation density [2].

The purpose of the present work is to present new measurements which are interpreted not only within Barnard's 3GM [2] but also using a new concept: a two-group model (2GM). The electrons on the Fermi surface are divided only into the following groups: electrons which are near to the Brillouin zone boundaries and electrons which are far away. Such a simplification corresponds better to the Watts model [8] of electron–dislocation scattering, where the dislocation resistivity is described by Bragg scattering of electrons lying very near to the Brillouin zone boundaries [9]. The division of the Fermi surface into different groups of electrons only has physical relevance if the variation of the ('real') average relaxation time (or

† Telephone: ++43-1-4277-514 44; fax: ++43-1-4277-514 40.

0953-8984/00/5010499+16$30.00

mean free path) of the electrons roughly follows the group boundaries. We will demonstrate that there are formal similarities of the temperature dependences of the DMR for deformed aluminium and that for deformed noble metals.

2. The DMRs in the two-group and three-group models

The temperature dependence of the experimental dislocation resistivity, $\rho_{\mathrm{d,ex}}(T)$, is written usually [10, 11] as

$$\rho_{\mathrm{d,ex}}(T) = \rho(T, \varepsilon) - \rho(T, \varepsilon = 0) \tag{1}$$

where $\rho(T, \varepsilon)$ and $\rho(T, \varepsilon = 0)$ are the resistivities of the deformed sample (with true strain ε; see section 3) and an undeformed reference sample at the measuring temperature T. Theoretically, $\rho(T, \varepsilon)$ and $\rho(T, \varepsilon = 0)$ are written as

$$\rho(T, \varepsilon) = \rho_{\mathrm{i}} + \rho_{\mathrm{p}} + \rho_{\mathrm{d}} + \delta_{\mathrm{ipd}} \tag{2}$$

$$\rho(T, \varepsilon = 0) = \rho_{\mathrm{i}} + \rho_{\mathrm{p}} + \delta_{\mathrm{ip}}. \tag{3}$$

Here ρ_{i}, ρ_{p} and ρ_{d} are the individual resistivity contributions of impurities, phonons and dislocations, δ_{ipd} is the DMR between impurities, phonons and dislocations and δ_{ip} is the DMR between impurities and phonons in the reference sample. Hence we get

$$\rho_{\mathrm{d,ex}}(T) = \rho_{\mathrm{d}} + \delta_{\mathrm{ipd}} - \delta_{\mathrm{ip}}. \tag{4}$$

For high-purity metals, $\delta_{\mathrm{ipd}} \gg \delta_{\mathrm{ip}}$ is usually valid [11] and therefore $\rho_{\mathrm{d,ex}}(T)$ reflects mainly the first DMR contribution. However, at low temperatures the case $\delta_{\mathrm{ipd}} < \delta_{\mathrm{ip}}$ is also possible, corresponding to a minimum in $\rho_{\mathrm{d,ex}}(T)$, as will be shown in this work (see section 4.4). We assume that at 4.2 K, δ_{ip} vanishes (as $\rho_{\mathrm{p}}(4.2) \approx 0$). From (4) it is clear that ρ_{d} (the so-called true dislocation resistivity which has at least a small difference from $\rho_{\mathrm{d,ex}}(4.2)$ even for high-purity metals) is not directly accessible to experiment and the DMRs in (4) have to be modelled.

For a description of the DMRs within a two-group model (2GM) [10], the three-scatterer DMR formula [11] developed for the noble metals can be taken over:

$$\delta_{123} = \left(\sum_{j=1}^{3} \rho_j \rho_{j+1} b A_{j+2} (A_j - A_{j+1})^2\right) \Bigg/ \left(\sum_{j=1}^{3} \rho_j (1 + bA_j)^2 A_{j+1} A_{j+2}\right). \tag{5}$$

δ_{123} is the DMR between three scatterers. The notation is cyclic with $\rho_4 \equiv \rho_1$, $\rho_5 \equiv \rho_3$, $A_4 \equiv A_1$, $A_5 \equiv A_2$, where A_j is the scattering anisotropy parameter and ρ_j is the resistivity of the jth scatterer. Instead of the neck and belly groups, we define the groups of electrons near to (N) and far from (F) the Brillouin zone boundaries. Then $b = \int_{\mathrm{N}} v \, \mathrm{d}S / \int_{\mathrm{F}} v \, \mathrm{d}S$ (cf. [12]), where v is the Fermi velocity and $\mathrm{d}S$ the Fermi surface element. A_j can be written as $A_j = \tau_{\mathrm{N}j}/\tau_{\mathrm{F}j}$, where $\tau_{\mathrm{N}j}$ and $\tau_{\mathrm{F}j}$ are the relaxation times in the near and far electron groups for the jth scatterer. It is emphasized that (effective) relaxation times for resistivity can also be defined at low temperatures where, additionally, small-angle electron–phonon scattering occurs. However, one is not allowed to use such relaxation times (or anisotropy parameters) for other transport properties [13].

In Barnard's 3GM [2, 6, 7], as described in the following, the Fermi surface is divided into a free-electron-like portion in the second zone, hole-like cylinders in the second zone just below the Brillouin zone boundaries and the electron-like monster in the third zone. Below 40 K the electron–phonon mean free paths in each group are characterized by [2]

$$l_{-}^{\mathrm{p}} = \gamma T^{-5} \qquad l_{++}^{\mathrm{p}} = \alpha T^{-3.3} \qquad l_{--}^{\mathrm{p}} = \beta T^{-2.8} \tag{6}$$

where $\alpha/\beta = 4.95$ and $\gamma/\alpha = 600$. The anisotropy parameters of the electron–impurity scattering are defined as (superscript i for impurities; subscripts $-$, $++$ and $--$ for the different groups)

$$a' = \frac{l^{\mathrm{i}}_{++}}{l^{\mathrm{i}}_{-}} \qquad b' = \frac{l^{\mathrm{i}}_{--}}{l^{\mathrm{i}}_{-}} \tag{7}$$

where according to [6] $a' = 1$ and $b' = 0.91$. Analogously, the anisotropy parameters a'' and b'' are defined for electron–dislocation scattering. Then, $\rho(T, \varepsilon)$ in (2) and $\rho(T, \varepsilon = 0)$ in (3) can be written as (cf. [2, 6])

$$\rho(\varepsilon, T) = (\rho_{\mathrm{i}} + \rho_{\mathrm{d}})\left(1 + \frac{y}{x}a^* + \frac{z}{x}b^*\right)\left[\frac{1}{1+F} + \frac{1}{1+G}\left(\frac{y}{x}a^*\right) + \frac{1}{1+H}\left(\frac{z}{x}b^*\right)\right]^{-1} \tag{8}$$

$$\rho(\varepsilon = 0, T) = \rho_{\mathrm{i}}\left(1 + \frac{y}{x}a' + \frac{z}{x}b'\right)\left[\frac{1}{1+F} + \frac{1}{1+G}\left(\frac{y}{x}a'\right) + \frac{1}{1+H}\left(\frac{z}{x}b'\right)\right]^{-1} \tag{9}$$

where x, y and z are band-structure terms proportional to the areas of the three regions of the Fermi surface and

$$a^* = a'(1+P)/(1+Q) \qquad b^* = b'(1+P)/(1+R) \tag{10}$$

where

$$P = \frac{\rho_{\mathrm{d}}(1 + (y/x)a'' + (z/x)b'')}{\rho_{\mathrm{i}}(1 + (y/x)a' + (z/x)b')} \qquad Q = a'P/a'' \qquad R = b'P/b''. \tag{11}$$

The details of the terms F, G and H can be found in [6] (the appropriate values of a^* and b^* or a' and b' have to be used). According to [6] we use $y/x = z/x = 0.4$ (a ratio of Fermi surface integrals similar to the term b in the 2GM). a^* is the mean anisotropy parameter of impurities and dislocations together, assuming that there is no contribution of the DMR between impurities and dislocations (this point was not mentioned by Barnard [2], and compared with a correct treatment of the DMR in the 3GM there will just be some shift in the fitted values of a'' and b'' which is not of great importance in our context). Equation (9) subtracted from (8) gives the description of $\rho_{\mathrm{d,ex}}(T)$ in the 3GM (see (1)).

In the high-temperature region (80 K to 300 K) where the resistivity varies linearly with temperature, we may assume that the electron–phonon scattering is isotropic (as for the noble metals) and that, therefore, the electron–phonon mean free paths are approximately equal. Then the terms F, G and H given in [6] simplify, e.g. for three scatterers (for two scatterers replace a^* by a' and b^* by b') to

$$F = \frac{\rho_{\mathrm{p}}}{\rho_{\mathrm{i}}}\left(1 + \frac{y}{x} + \frac{z}{x}\right)\left(1 + a^*\frac{y}{x} + b^*\frac{z}{x}\right)^{-1} \qquad G = a^*F \qquad H = b^*F. \tag{12}$$

3. Experimental details

The samples were prepared from rods (diameter 6 mm) of 99.9999% pure aluminium (MATERIAL RESEARCH S.A.). According to the analysis certificate, the significant impurities were Si (1 ppm), Mg (0.8 ppm) and Ca (0.4 ppm). Pieces of 35 mm length were cut and rolled to sheets of different thicknesses (suited to getting, after the final deformation, samples with thickness of approximately 200 μm). The sheets were annealed in high vacuum ($p < 3 \times 10^{-3}$ Pa) at 380 °C for ten hours and had then an impurity resistivity (residual resistivity at 4.2 K) $\rho_{\mathrm{i}} = 0.58$ nΩ cm. The mean grain size seen on the surface of the sheets was $\approx$400 μm.

The dislocations were introduced into the annealed sheets by rolling in steps of ≈10% strain up to the desired ε-value: $10\% < \varepsilon < 160\%$ (true strain: $\varepsilon = \ln(d_0/d)$; d_0 is the initial and d is the final thickness of the sample). The final arm-shaped samples ($45 \times 3 \times 0.2$ mm^3) were cut by spark erosion (for details see [14]). Electrical contact to the samples was made by means of spot-welded high-purity aluminium wires (0.25 mm diameter). The samples were stored in liquid nitrogen. The total exposure at room temperature of the arm-shaped samples between the introduction of dislocations and the DMR measurement was ≈50 h.

For the isochronal and isothermal annealing experiments, separate samples in the form of strips ($35 \times 3 \times 0.4$ mm) were prepared (with $\rho_i = 0.48$ nΩ cm; this value is slightly lower than for the arm-shaped samples, as the strips had approximately twice the thickness and therefore the surface contamination caused by rolling was reduced). The strips were quenched immediately after the rolling process into liquid nitrogen and were mounted into the sample holder in liquid nitrogen (press contacts). The isothermal annealing was performed at room temperature. The holding time for the isochronal annealing was seven minutes; the temperature was varied in 10 K steps. Temperatures between −160 °C and +20 °C were realized by varying the position of the sample holder in the neck of the helium can (accuracy of temperature: ±1 K). Annealing at the temperatures from +30 °C to 140 °C was performed in an oil bath (accuracy: ±0.1 K). The resistance of the samples between the various isothermal and isochronal annealing states was always measured in liquid helium at 4.2 K with a resolution of 1 nV.

The temperature dependence of the resistance of the deformed samples was always measured together with that of an undeformed reference sample in an evaporation cryostat as described elsewhere [11]. The geometry factor G was determined from the relation (RT is the room temperature)

$$G = \frac{R(\mathrm{RT}) - R(4.2\ \mathrm{K})}{\rho_p(\mathrm{RT})}. \tag{13}$$

Here R(RT) and R(4.2 K) are the resistance values of the undeformed samples (reference samples) or of annealed deformed samples (after doing the required measurements). ρ_p(RT) is the ideal phonon resistivity of aluminium at room temperature [15] and was interpolated from the values at 273.15 K and 295 K. The deformed samples were annealed for six hours at 380 °C, where the resistivity values of the reference samples agreed well (±0.1 nΩcm) with the resistivity values of the annealed samples. The experimental dislocation resistivity is obtained from (1).

4. Results and discussion

4.1. The experimental dislocation resistivity at 4.2 K and the annealing behaviour of dislocations

Figure 1 shows the experimental dislocation resistivity $\rho_{d,ex}(T)$, at $T = 4.2$ K, 77 K and 125 K, as a function of the deformation ε. The beginning of the curve at 4.2 K agrees well with the data of Wintenberger [16] for 99.999% pure aluminium. The maximum at $\varepsilon = 65\%$ (for 4.2 K and 77 K) arises from the fact that in high-purity aluminium dislocations are already partially annealed at room temperature as will be shown below. For 125 K the maximum is shifted to $\varepsilon = 91\%$ by the higher DMR contributions at 125 K.

The results of our separate isochronal and isothermal annealing investigations are represented in figure 2 and figure 3. The isochronal curves (figure 2) show the typical two-stage annealing [4, 17]. The first rapid decreases of the resistivity curves are very similar for all four samples, starting at −70 °C and stemming from the annealing of vacancies (first stage). The

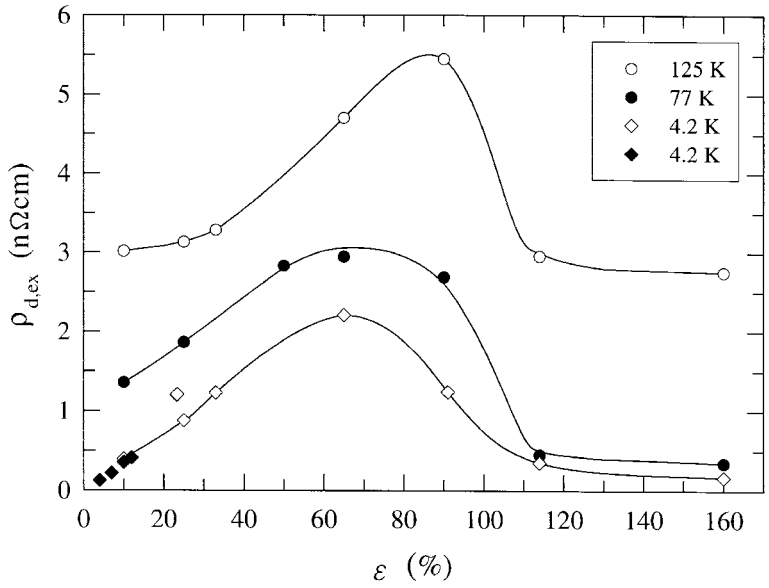

Figure 1. The experimental dislocation resistivity $\rho_{d,ex}(T)$ at $T = 4.2$ K, 77 K and 125 K as functions of the deformation ε. Diamonds: data from Wintenberger [16].

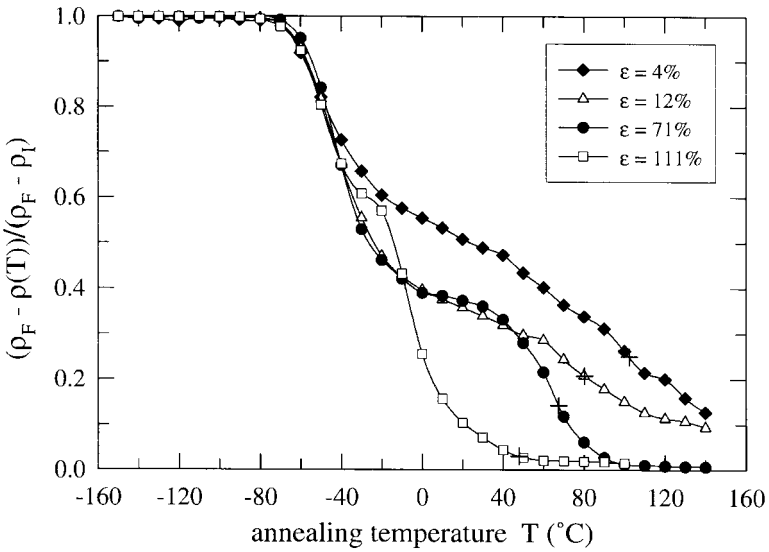

Figure 2. Isochronal annealing after rolling and quenching to 77 K. $\rho_F = 0.48$ nΩ cm (final resistivity); ρ_I (initial resistivity) has the values 1.77, 4.69, 11.90 and 17.40 nΩ cm for the ε-values 4, 12, 71 and 111%, respectively. Note: ρ_F, ρ_I and $\rho(T)$ were measured at 4.2 K.

second rapid decrease (second stage) is shifted to lower temperatures with increasing ε-value and lies in the range $-20\,^{\circ}$C ($\varepsilon = 111\%$) to $+40\,^{\circ}$C ($\varepsilon = 4.5\%$). This second stage originating from the annealing of dislocations becomes more visible as ε (or the initial dislocation density) becomes higher.

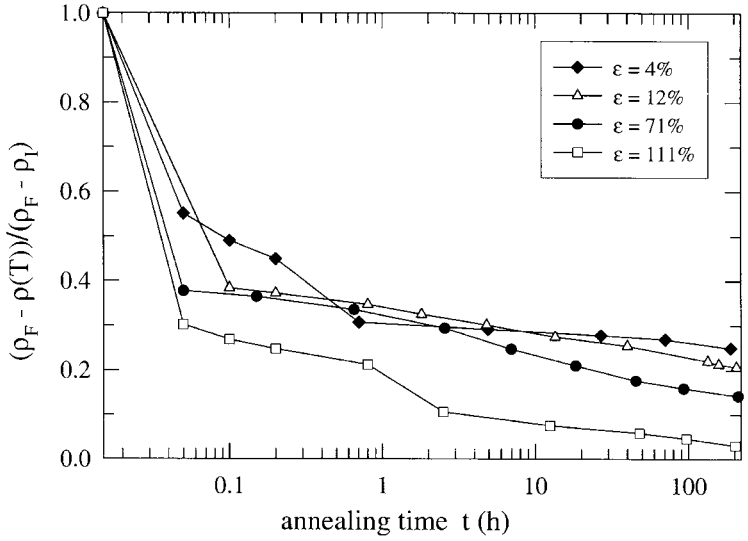

Figure 3. Isothermal annealing after rolling and quenching to 77 K at room temperature (≈298 K). $\rho_F = 0.48$ nΩ cm; ρ_I has the values 2.022, 5.124, 12.140 and 16.947 nΩ cm for the ε-values 4, 12, 71 and 111%, respectively.

The isothermal annealing curves at room temperature (figure 3) show the largest resistivity decrease within the first six minutes. After three hours the resistivity decreases only rather slowly. However, the higher the deformation, the lower the level that the curves reach. In particular, the curve for $\varepsilon = 111\%$ lies significantly lower than the other curves. The values of the isothermal curves at 200 hours (out of range in figure 3) are marked by crosses on the related isochrones of figure 2. Hence, it can be concluded that during handling and storage of the samples at room temperature, a considerable number of dislocations are lost (especially if $\varepsilon > 70\%$). As the loss of dislocations is larger at higher values of deformation, each curve of the experimental dislocation resistivity in figure 1 shows a maximum.

For high-purity metals the discrepancy between $\rho_{d,ex}(4.2)$ and ρ_d is small (<0.06 nΩ cm for the present samples; see section 4.3). As ρ_d is proportional to the length of the dislocation line [9, 18] and rather insensitive to the dislocation arrangement [19] and the long-range strain field [20], it will be a measure of the dislocation density. Thus, from $\rho_{d,ex}(4.2)$ given in figure 1, the dislocation density due to electrical measurements, N_e, can already be calculated:

$$N_e = \rho_{d,ex}(4.2)/R_d \tag{14}$$

where $R_d = 1.1 \times 10^{-25}\ \Omega\ m^3$ is the experimental value of the specific dislocation resistivity of aluminium after [8]. The result is shown by the open circles in figure 4. For comparison, the dislocation density obtained by x-ray Bragg profile analysis (N_x) for comparable 99.9999% pure aluminium samples after [21] is also plotted in figure 4. It can be seen that the x-ray method 'sees' the same maximum in the dislocation density as the electrical resistivity and that the values of N_e and N_x agree well within the errors. Here it should be noted that agreement between N_e and N_x was not found for copper [22] and dilute copper–gold alloys [14], where for $\varepsilon > 40\%$ the N_x-values are only 60% of the N_e-values. The higher dislocation density from the electrical measurements was interpreted as reflecting the fact that the XPA method does not usually 'see' dislocation loops with a diameter smaller than 5 nm. Since copper has a low stacking fault energy [23], deformation-induced vacancies can agglomerate and form

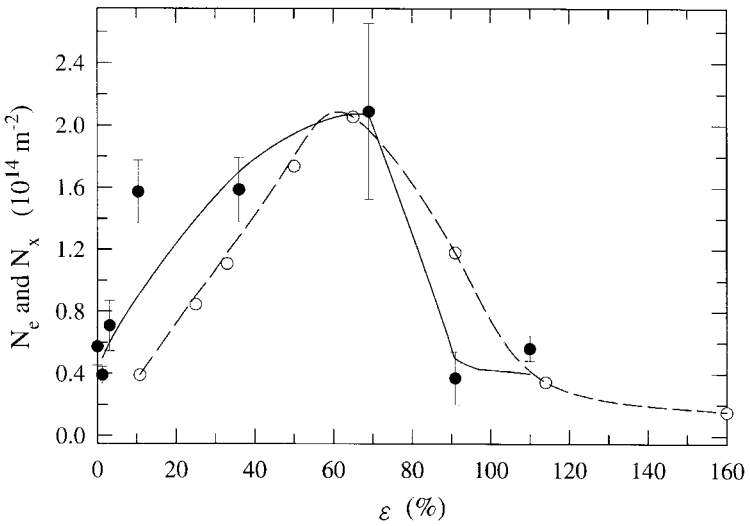

Figure 4. Comparison of the dislocation densities from electrical measurements (N_e; open circles) and from XPA (N_x; full circles).

small dislocation loops. In contrast, aluminium has a high stacking fault energy [23] which impedes the formation of small dislocation loops from deformation-induced vacancies. As shown in figure 2, the vacancies can anneal far below room temperature.

4.2. The temperature dependence of the experimental dislocation resistivity

In order to eliminate a possible systematic error in the shape factor, we use the normalized experimental dislocation resistivity $D(T)$ given as (see (4))

$$D(T) = \frac{\rho_{d,ex}(T)}{\rho_{d,ex}(4.2)} = \frac{\rho_d + \delta_{ipd}(T) - \delta_{ip}(T)}{\rho_d + \delta_{ipd}(4.2) - \delta_{ip}(4.2)}. \tag{15}$$

Since $\delta_{ip}(4.2) \approx 0$ and $\delta_{ipd}(4.2) \approx \delta_{id}(4.2)$, equation (15) yields approximately

$$D(T) \approx \frac{\rho_d + \delta_{ipd}(T) - \delta_{ip}(T)}{\rho_d + \delta_{id}(4.2)} \tag{16}$$

where $\delta_{id}(4.2) \ll \rho_d$ (and therefore the difference between $\rho_{d,ex}(4.2)$ and ρ_d is small; see section 4.3). The full temperature dependence of the normalized experimental dislocation resistivity $D(T)$ can be seen in figures 5(a), 5(b) (surveyed up to room temperature) and figure 6 (details below 35 K). The qualitative behaviour of the data (symbols in figure 5) is comparable to that of the noble metals [12, 24]: there is a rapid increase of the DMR in the temperature range from 25 K to 125 K and then the DMR levels off. However, while for the noble metals the values $D(300)$ are between 1 and 2 [11], for the aluminium samples considered, a range between 2 and 20 is covered. As an example, $D(125)$, which corresponds roughly to $D(300)$, and $D(77)$ are shown in figure 7. According to Watts (p 399 of [8]), the decrease of the normalized dislocation resistivity (at a fixed temperature) with increasing $\rho_{d,ex}$ has a natural explanation: the curves in figure 7 follow mainly the ratio $\rho_p(T)/\rho_d$ (where T is constant); however, there is also some influence of $A_p(T)$ (which may be assumed to be unity at 125 K) and the geometry of the Brillouin zone and of the Fermi surface (which determines the anisotropy of the electron–dislocation scattering).

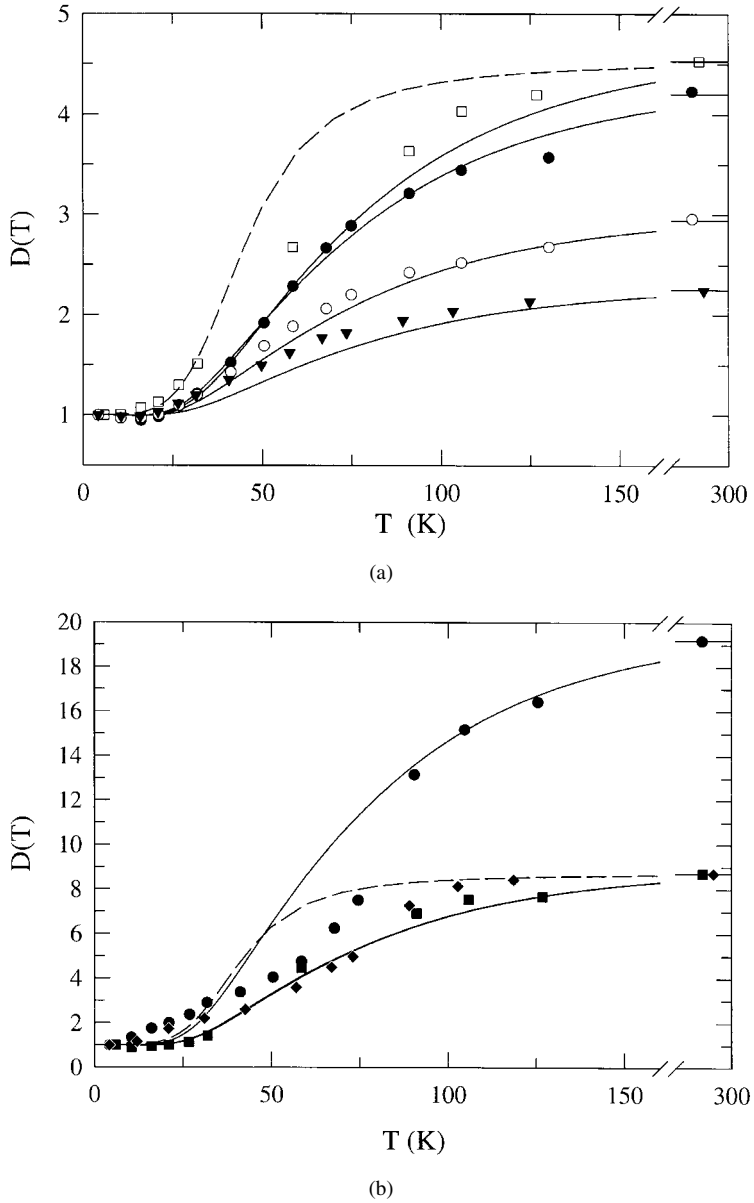

Figure 5. Normalized dislocation resistivity $D(T)$ as a function of temperature from 4.2 K to 300 K. Symbols: experimental data; full lines: DMR fits made by adjusting A_d and ρ_d (using (17) and (18)) with anisotropic A_p-values; dashed lines: DMR fits like the full lines but with $A_p = 1$. (a) Full circles: $\varepsilon = 25\%$; open circles: $\varepsilon = 33\%$; triangles: $\varepsilon = 65\%$; squares: $\varepsilon = 91\%$. (b) Squares: $\varepsilon = 10\%$; diamonds: $\varepsilon = 114\%$; circles: $\varepsilon = 160\%$. Note: the full lines for 10% and 114% coincide.

In the low-temperature region (figure 6) a minimum occurs for deformations between 10% and 65%, where the depth of the minimum decreases with increasing dislocation resistivity (compare figure 1). Although for the samples with 114% and 160% deformation the dislocation resistivity is comparable (114%) or smaller (160%) than that for the sample with 10%

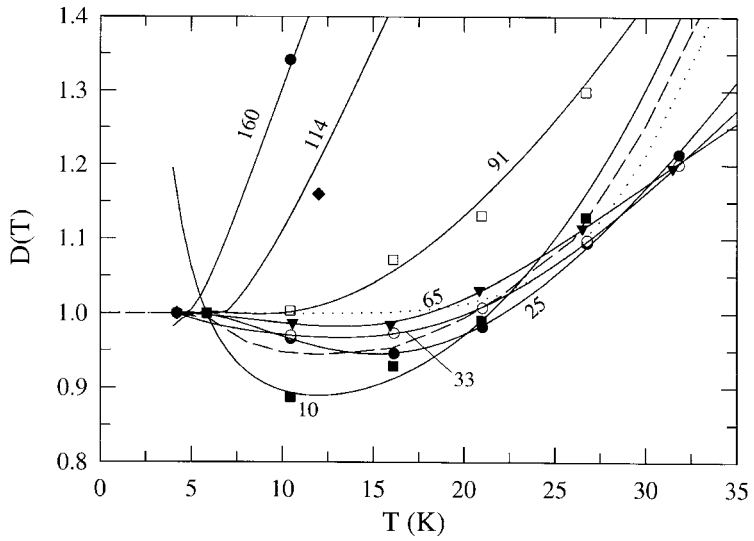

Figure 6. Normalized dislocation resistivity $D(T)$ as a function of temperature from 4.2 K to 35 K. Symbols: experimental data; full lines: mathematical curves fitted to the experimental data; dashed curve: 2GM fit of the 25% sample with the exact-fit data for the 10% sample (with $A_d = 0.07$, $A_i = 1.2$ and $A_p(10\%)$; see table 1); dotted line: 2GM fit for the 114% sample with $A_d = 0.07$, $A_i = 0.1$ and $A_p(10\%)$; see the text.

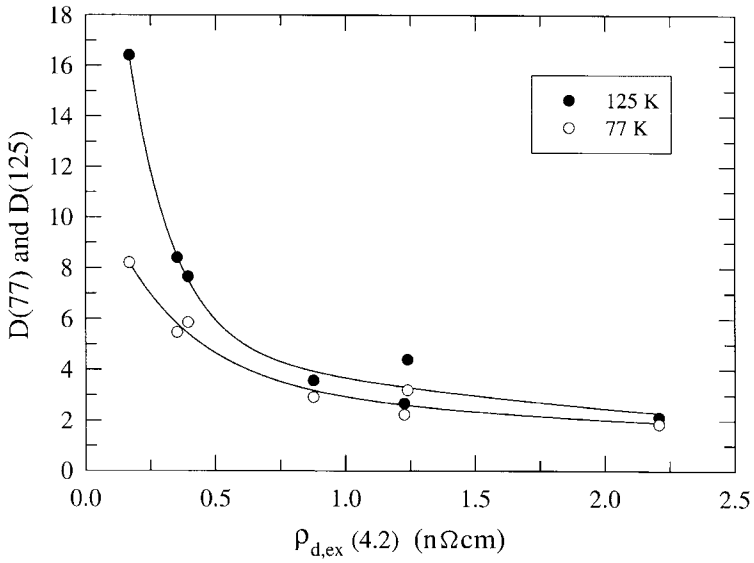

Figure 7. Normalized dislocation resistivities $D(77)$ and $D(125)$ as functions of the experimental dislocation resistivity $\rho_{d,ex}(4.2)$.

deformation (compare figure 1), the curves for the two former samples show a steep increase instead of a minimum. Qualitatively, the behaviour of the curves in figure 6 is comparable to that in figure 2 of the work of Endo *et al* [1] which shows DMR curves for drawn wires of 99.9999% pure aluminium. Endo *et al* also found that samples with approximately the same dislocation

Table 1. Anisotropy parameters for electron–phonon scattering (see the text).

T (K)	A_p(Al)	a^p	b^p	Al(10%)	Al(114%)
6	0.28	0.035	0.017	0.013	71
10	0.30	0.084	0.053	0.025	61
16	0.33	0.19	0.15	0.18	13
20	0.36	0.27	0.25	0.43	4.7
26	0.41	0.42	0.44	0.64	2.0
30	0.44	0.54	0.60	0.79	1.63
36	0.49	0.74	0.89	0.97	1.47
40	0.52	0.88	1.13	1.11	1.46
50	0.60	1.29	1.84	1.54	1.56

resistivity can show either a minimum (slightly deformed sample) or a steep increase in the DMR curve if the dislocation density after deformation was lowered by annealing (e.g., at 200 °C for 30 minutes). However, Endo *et al* [1] also observed the annihilation of dislocations due to holding the samples at room temperature, as is found in the present investigation.

4.3. Step-height fits with the two-group and three-group models

We define the step height of the temperature dependence of the normalized dislocation resistivity as $D(280\ \mathrm{K}) - 1$ (the difference in $D(T)$ between 280 K and 4.2 K). Then the true dislocation resistivity ρ_d and the appropriate anisotropy parameter A_d can be calculated within the 2GM by using the following two fitting conditions for the experimental data:

$$\rho_{d,ex}(4.2) = \rho_d + \delta_{id}(4.2) \tag{17}$$

$$D(280) = \frac{\rho_{d,ex}(280)}{\rho_{d,ex}(4.2)} = \frac{\rho_d + \delta_{ipd}(280) - \delta_{ip}(280)}{\rho_d + \delta_{id}(4.2)} \tag{18}$$

where $\delta_{id}(4.2)$, $\delta_{ipd}(280)$ and $\delta_{ip}(280)$ are described by (5), relating the subscripts 1, 2, 3 to i, p, d (standing for impurities, phonons and dislocations). We use:

(i) $\rho_i = 0.58\ \mathrm{n\Omega\,cm}$ and $A_i = 1$, as Barnard estimated the anisotropy of the electron–impurity scattering to be near unity [6]. Here it should be noted that anisotropy parameters or ratios to the mean free path (l) differ from ratios to the relaxation time (τ) by a factor that is the ratio of the Fermi velocities (v), as $l = v\tau$ for each group. Since we want to show only the relative importance of the anisotropy parameters, we may assume $v = 1$ (in free-electron units).

(ii) ρ_p as the ideal phonon resistivity of aluminium, after [15], and A_p as a function of temperature derived in the following way: the temperature scale of the rather reliable A_p-curve for copper [24] was multiplied by $\Theta(\mathrm{Al})/\Theta(\mathrm{Cu})$ in order to adapt the A_p-curve to the actual Debye temperature (Θ). We used $\Theta(\mathrm{Al}) = 428$ K and $\Theta(\mathrm{Cu}) = 346$ K [25]. Values of this adapted curve are indicated as A_p(Al) in table 1.

(iii) ρ_d and A_d fitted.

(iv) $b = 0.15$ as a reasonable assumption compared to $b = 0.15$ to 0.219 for the noble metals.

Having A_d and ρ_d fixed by (17) and (18), the whole temperature dependence of $D(T)$ given by (16) can be calculated for each sample investigated. The results are shown by the solid curves in figures 5(a) and 5(b). It can be seen that the fits for the samples with 10%, 25%, 33% and 65% deformation are quite close to the experimental points, whereas for the samples with 91%, 114% and 160% deformation, larger deviations occur. This is a similar behaviour

to that found for the noble metals [11, 24]. If $A_p = 1$ is chosen for the fits (dashed curves in figures 5(a) and 5(b)), the discrepancy from the experimental data gets significantly larger. Thus our adaptation of the A_p-curve of copper to aluminium is reasonable.

The fitted values of A_d are plotted in figure 8 as a function of the deformation. In addition to the fit with $b = 0.15$ we performed the fits within the 2GM also with $b = 0.277$ and $b = 0.1$ (not shown). The A_d-values obtained are proportional to $\rho_{d,ex}(4.2)$ (cf. figure 1) and to the selected value of b. Here it should be noted that the quality of the step-height fits shown in figure 5 is influenced only very slightly by which value of b is considered. $b = 0.277$ was chosen, because with this value, at the maximum dislocation resistivity ($\varepsilon = 65\%$) the value $A_d = 0.1$ is reached, which is a typical value for the noble metals [12]. The variation of the A_d-values of the present aluminium samples is substantially comparable with that of copper samples having $\rho_{d,ex}(4.2)$ also in the range 0 to 2.5 nΩ cm [11, 26]. In this range for high-purity copper, typically $0.05 < A_d < 0.1$ was found [11], whereas our fits for aluminium require typically $0.01 < A_d < 0.1$. However, for copper with $\rho_i \approx 0.6$ nΩ cm and with rather small A_i-values, a constant or decreasing variation of A_d with the dislocation resistivity was also found [11]. We checked (not shown) that, unlike the case for copper, the principal behaviour of the A_d-curves in figure 8 remained the same independently of the choice of usual A_i-values in the range 0.1 to 3. For $b = 0.15$, 0.1 or 0.277, the fitted values of ρ_d are typically 0.06, 0.04 or 0.1 nΩ cm lower, respectively, than the values of $\rho_{d,ex}(4.2)$. Therefore the ρ_d-values are not represented.

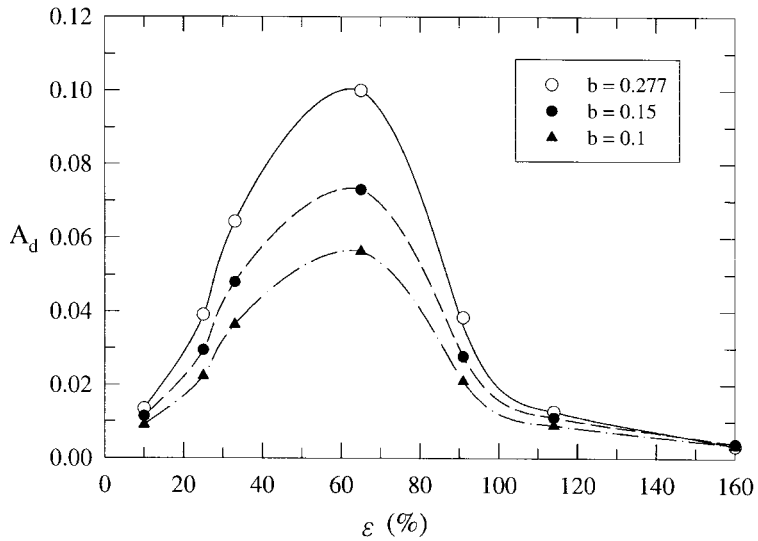

Figure 8. The anisotropy parameter A_d obtained from 2GM fits with different b-values, as functions of the deformation.

For the step-height fit within the 3GM we put the right-hand sides of (8) and (9) with the terms F, G and H based on (12) into (1), i.e. we assume isotropic electron–phonon scattering. The electron–impurity scattering is assumed to be nearly isotropic with $a' = 1$ and $b' = 0.91$ after [6]. For simplicity we assume for the anisotropy parameters a'' and b'' of electron–dislocation scattering the relation $b'' = 2a''$. The values of a'' needed (3GM) to describe the experimental step height (cf. figure 5) are plotted in figure 9 together with the values of A_d (2GM) as functions of the dislocation resistivity. It can be seen that the strong increase of the anisotropy parameters (either A_d or a'') with $\rho_{d,ex}(4.2)$ is in principle independent of the

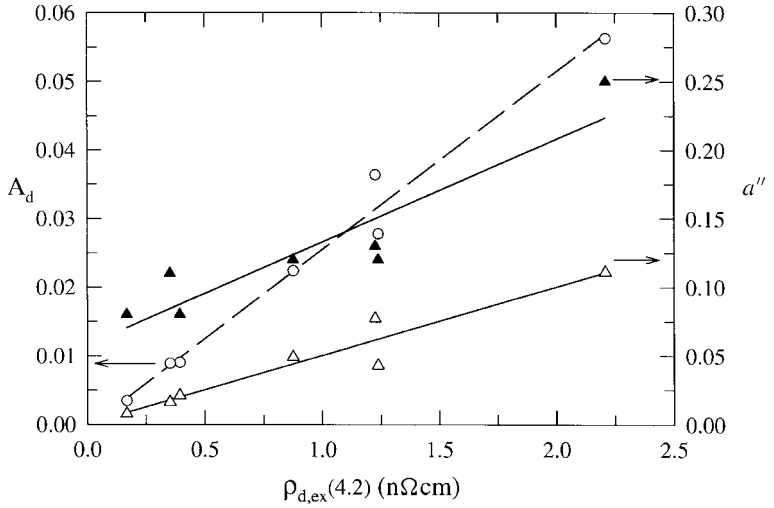

Figure 9. Comparison of the anisotropy parameters from fits within the 2GM (A_d: open circles and dashed line) and the 3GM (a'': triangles and full lines,). Open triangles: the step-height fit in the 3GM with isotropic electron–phonon mean free paths; full triangles: the precise curve fit (3GM) in the range 4.2 K to 40 K based on (6) to (11).

model used. As for the noble metals, the increase of A_d (and analogously of a'') found from the step-height fits seems to be due to the inaccuracy of the models (e.g. neglect of small-angle scattering processes [24]) which is clearly visible as long as the dislocations are not the dominating scatterers. For larger values of $\rho_{d,ex}(4.2)$, we expect for aluminium anisotropy parameters of the electron–dislocation scattering independent of the dislocation density, as for the noble metals [11, 12].

4.4. The DMR minimum at low temperatures

As shown in [2], the 3GM is able to describe the experimental DMR curves below 40 K very well. Also the present DMR curves of figure 6 are described well by the 3GM. So we do not represent the curves fitted by the 3GM (equations (6) to (11)); we discuss only the parameters a'' and b'' needed. According to Barnard [2], a'' should be the smaller anisotropy parameter; thus this would be in line with the case for noble metals ($A_d \leqslant 0.15$ for pure metals; see [11, 12]), where the relaxation times for hole-like states near the Brillouin zone boundaries are relatively small compared with those for the nearly free-electron belly states. Using this idea, we obtained the a''-values represented by the full triangles in figure 9. These values are comparable to the A_d-values for the noble metals [11, 12] and are only in some cases larger than the A_d-values of the step-height fits in the 2GM. However, then for b'' (not shown), values in the range 0.3 (10%) up to 2 (91%) are needed, similarly to in Barnard's fits [2]. For the samples with $\varepsilon = 114\%$ and 160% we even need $b'' = 8$ and 15, respectively. Here it should be noted that a near interchange of a'' and b'' also gives acceptable fits, as y/x and z/x have the same value 0.4 and the temperature dependences of the mean free path l^p_- and l^p_{++} are similar. Furthermore, we point out the following: in Barnard's 3GM, the anisotropy of the electron–phonon scattering is fixed by (6). Therefore some stronger variation in b'' (or a'') is needed when the deformation is increased. For the noble metals there is a similar situation: A_d is usually kept constant and it is evident that with increasing deformation a severe correction of the electron–phonon scattering is needed [11, 24].

Strictly speaking, Barnard's model is more a 2GM than a 3GM (as $y/x = z/x$, $a' \sim b'$ and the types of electron–phonon scattering in the second and third groups are rather similar; see table 1). In the following we show that the formalism of the 2GM as used for the noble metals is also able (and sufficient) to explain the DMR minima (figure 6) of our deformed aluminium samples. As can be checked easily by trial and error, the condition for a minimum within the 2GM based on the three-scatterer formula (5) is that the three anisotropy parameters are different and that (for instance) the dislocation resistivity is small enough.

According to figure 8 (the curve with $b = 0.15$), we fixed $A_d = 0.07$ for dominant electron–dislocation scattering. $A_i = 1.2$ was chosen, since we found from our fits for the curves in figure 6 that the A_i-value fixes the depth of the minimum for the sample with the smallest deformation. Smaller A_i-values would decrease and larger A_i-values would increase the depth of the minimum. Some of the A_p-values required (together with $A_d = 0.07$ and $A_i = 1.2$) to fit our 10% curve exactly in the range 4 K to 50 K (figure 6) are given in table 1 (indicated as $A_p(10\%)$). Hence, the fit of the 10% curve in the 2GM is identical with the solid line for the 10% sample in figure 6. As $D(T)$ is defined by (16), a minimum within the 2GM calculation can only arise if $\delta_{ipd} < \delta_{ip}$ in the numerator of (16). Additionally, table 1 shows the anisotropy parameters $a^p = l^p_{++}/l^p_-$ and $b^p = l^p_{--}/l^p_-$ calculated from the temperature dependence of the electron–phonon mean free paths given by (6).

Now the description of the 25% curve is obtained (the dashed line in figure 6) by taking just the value of $\rho_{d,ex}(4.2)$ for the 25% sample and using all the other parameters for the 10% sample unchanged (i.e. the $A_d = 0.07$, $A_i = 1.2$ and Al(10%) of table 1). Similarly, the depth of the flatter minima can be obtained by varying only $\rho_{d,ex}(4.2)$ (not shown for clarity in figure 6). However, it is impossible to describe even roughly the rapidly increasing curves of the 114% and 160% samples with the parameters used before. Since $\rho_{d,ex}(4.2)$ for the 114% sample is comparable to $\rho_{d,ex}(4.2)$ for the 10% sample, we would obtain a minimum too (the same is true for the 160% sample). We have found that the change from a DMR curve with a minimum to a monotonically increasing DMR curve (like the 10% and 114% ones, for which we have approximately the same value of $\rho_{d,ex}(4.2)$) can only be described if A_i is reduced to near the value of A_d (e.g. $A_d \sim 0.07$ and $A_i \sim 0.1$ yields the dotted curve for 114% in figure 6, where the values of $A_p(10\%)$ of table 1 were used).

In principle, a change of A_i would be possible if during the annealing of dislocations (the problem concerns only samples with a large proportion of annealed dislocations), the impurity atoms are built into the edge dislocation lines. As edge dislocations have a defined relation to certain lattice directions, the scattering anisotropy of the impurities could be changed. Otherwise, this idea with $A_d \sim A_i \sim 0.1$ (or 0.2) is not able to explain the rapid increase for the 91%, 114% and 160% curves. Interestingly, the major impurities in our material (see section 3) are well suited to being built into edge dislocations: Mg and Ca have larger atoms than Al, whereas Si has smaller atoms [27].

We suggest that it is a better solution to keep $A_d = 0.07$ and $A_i = 1.2$ fixed and to adjust A_p. Then with one set of A_d and A_i, all the curves in figure 6 (either with minimum or rapid increase) can be formally described. In order to show the range of A_p-values necessary to describe exact fits within the 2GM, A_p-values for the 10% and 114% samples are listed in table 1 (indicated as Al(10%) and Al(114%)), where they can be compared with the values of a^p and b^p calculated using (6). Obviously, for the 114% sample the A_p-values are much larger than unity, while the A_p-values for the 10% sample are comparable with the values of a^p and b^p. We think that this behaviour is in line with that of the noble metals, where for samples with higher deformation, A_p-values larger than unity are needed below 50 K [24]. However, one has to bear in mind that aluminium has *a priori* a larger anisotropy for electron–phonon scattering.

The physical interpretation of the significant increase of the fitted A_p-values with deformation could be the following: the ideal phonon resistivity below 20 K or 30 K is dominated by small-angle scattering [13]. Certainly we can assume that the lattice vibrations around a dislocation line are somewhat modified ('local phonon modes'). Such phonons will be 'seen' by the conduction electrons with a somewhat increased scattering cross section as long as the electron mean free path L_p is much larger than the mean distance a between two dislocation lines. Since the Burgers vectors of the edge dislocations (in aluminium there are mainly edge dislocations for $\varepsilon > 30\%$; see e.g. [28, 29]) are typically in [011] directions [30], we expect that for the electron–phonon scattering there arises a strong scattering anisotropy; i.e. electrons having their k-vectors in [011] directions should be scattered more strongly. In terms of the noble metals, this would mean that the belly electrons are scattered more strongly by local phonon modes than the neck electrons. For our 10% and 114% samples we estimated from figure 4 ($N \sim 0.4 \times 10^{14}$ m^{-2}) $a \sim 0.1$ μm, while $L_p \sim 40$ μm for $T \approx 22$ K (free-electron estimation for aluminium with an ideal resistivity of 1 nΩ cm after [13]). Thus, $a \ll L_p$ is in general valid, say for $T \leqslant 40$ K (also for copper). For aluminium we have $a \leqslant L_p$ up to a resistivity $\rho_p = 400$ nΩ cm, which corresponds to a temperature of $\approx$95 K. Although the idea of local phonon modes [31] has been mentioned often [32–34], in the context of DMR it has not really been successful up to now [8, 34]. Unlike other authors, we suggest that the high scattering anisotropy of lattice vibrations modified by dislocations gives rise to a considerable DMR contribution (based mainly on small-angle scattering). Additionally, impurities built into dislocation lines could enhance the effect of local modes. As $L_p < a$ above 100 K, we expect the role of the 'local modes' to become negligible, as the usual large-angle electron–phonon scattering will clearly dominate. The existence of special phonon modes at edge dislocations was asserted recently [35].

5. Conclusions

The investigation of the electrical dislocation resistivity and of the dislocation density in high-purity aluminium is complicated by the fact that dislocations are already partially annealing out at room temperature. The higher the initial dislocation density, the larger the effect of room temperature annealing of dislocations. So, slightly deformed samples (having lost almost no dislocations) and highly deformed samples (with a high proportion of annealed dislocations) can have comparable values of the dislocation resistivity or dislocation density. Such samples can be clearly distinguished by the temperature dependence of the experimental dislocation resistivity (DMR) at low temperatures (4.2 K $< T <$ 50 K). A minimum in the DMR occurs for samples with strain $\varepsilon \leqslant 65\%$ where the annihilation effect of dislocations at room temperature is moderate. For larger (nominal) strains, a monotonic increase of the DMR is found which gets steeper with increasing strain, i.e. steeper with increasing number of annealed dislocations. However, the two types of DMR curve cannot be distinguished by their step heights at high temperature: the normalized step height (e.g. D(125 K)) lies on one curve which decreases with the measured dislocation resistivity independently of the sample history (figure 7).

The step height of the DMR curves and the principal behaviour of the curves below 40 K can be described either with a three-group model or with a two-group model. The description with the two-group model has the advantage that the anisotropy parameters needed for the electron–dislocation scattering are always much smaller than unity (even in the region of the DMR minima). Thus, qualitative agreement with the Watts model of dislocation resistivity is achieved within the 2GM, while in general this is not the case for the 3GM (also, anisotropy parameters for the electron–dislocation scattering larger than unity are obtained). Furthermore, fits of the temperature dependence of the experimental dislocation resistivity in the two-group

model show clearly that the principal physics of the DMR in aluminium is comparable to that for the noble metals. However, the anisotropy of the electron–phonon scattering at low temperatures is considerably larger in aluminium. If the anisotropy parameters for electron–dislocation and electron–impurity scattering are fixed (large-angle scattering) for the whole set of samples, then, as found for the noble metals, A_p (small-angle scattering) is a function of the (nominal) deformation. The change of A_p could arise from modified phonon modes at edge dislocation lines (which are prominent in the present samples). Since these dislocations are bound to certain lattice directions, local phonon modes could give rise to more or less scattering anisotropy depending on the deformation state and annealing state. In samples where a high proportion of the dislocations are already annealed, impurities built into the dislocation lines could enhance the effect of local phonon modes. This could be one reason for the rapid increases of the DMR curves for the 114% and 160% samples.

Acknowledgments

Helpful discussions with V Gröger, M Zehetbauer and B R Watts are gratefully acknowledged. This work was supported by the Austrian Fonds zur Förderung der wissenschaftlichen Forschung under projects 9930-PHY and 12945-PHY.

References

[1] Endo T, Sasaki K and Kino T 1985 *J. Phys. F: Met. Phys.* **15** 1963
[2] Barnard R D 1986 *J. Phys. F: Met. Phys.* **16** 203
[3] Kino T, Endo T and Kawata S 1974 *J. Phys. Soc. Japan* **36** 698
[4] Schmidt J 1990 *Thesis* Technische Universität Braunschweig
[5] Haessner F and Schmidt J 1988 *Scr. Metall.* **22** 1917
[6] Barnard R D and Abdel Rahiem A E E 1980 *J. Phys. F: Met. Phys.* **10** 2749
[7] Barnard R D 1980 *J. Phys. F: Met. Phys.* **10** 2739
[8] Watts B R 1989 *Dislocations in Solids* vol 8, ed F R N Nabarro (Amsterdam: Elsevier)
[9] Watts B R 1988 *J. Phys. F: Met. Phys.* **18** 1197
[10] Sachslehner F 1994 *J. Phys.: Condens. Matter* **6** 11 229
[11] Zürcher R, Müller M, Sachslehner F, Gröger V and Zehetbauer M 1995 *J. Phys.: Condens. Matter* **7** 3515
[12] Sachslehner F 1995 *J. Phys.: Condens. Matter* **7** 3913
[13] Ashcroft N W and Mermin N D 1976 *Solid State Physics* (New York: Saunders)
[14] Sachslehner F, Milnera M, Kocer M and Schafler E 2000 *Phys. Status Solidi* a **179** 407
[15] Bass J 1982 *Landolt–Börnstein New Series* Group III, vol 15a, ed K-H Hellwege and J L Olsen (Berlin: Springer) p 15
[16] Wintenberger M 1959 *Acta Metall.* **7** 549
[17] Ceresara S, Elkholy H and Federighi T 1965 *Phil. Mag.* **12** 1105
[18] Bross H and Häberlen O 1993 *J. Phys.: Condens. Matter* **5** 7687
[19] Watts B R 1987 *J. Phys. F: Met. Phys.* **17** 1703
[20] Watts B R 1988 *J. Phys. F: Met. Phys.* **18** 1183
[21] Schafler E 1998 *Thesis* Universität Wien
[22] Müller M, Zehetbauer M, Borbély A and Ungár T 1995 *Proc. EUROMAT '95: 4th European Conf. on Advanced Materials and Processes (Padua/Venice, Italy)* p 305
[23] Massalski T B 1996 *Physical Metallurgy* vol 1, 4th edn, ed R W Cahn and P Haasen (Amsterdam: North-Holland) p 191
[24] Sachslehner F 1996 *J. Phys.: Condens. Matter* **8** 5891
[25] Schober H R and Dederichs P H 1981 *Landolt–Börnstein New Series* Group III, vol 13a, ed K-H Hellwege and J L Olsen (Berlin: Springer) p 10
[26] Müller M 1994 *Thesis* Universität Wien
[27] King H W 1966 *J. Mater. Sci.* **1** 79
[28] Haasen P 1994 *Physikalische Metallkunde* 3rd edn (Berlin: Springer)

[29] Schafler E, Zehetbauer M and Ungár T 2000 *Proc 12th Conf. on Strength of Materials (Monterey, CA, USA, 27 August–1 September 2000); Mater. Sci. Eng.* A at press
[30] Hull D and Bacon D J 1984 *Introduction to Dislocations* 3rd edn (Oxford: Pergamon) p 91
[31] Gantmakher V F and Kulesko G I 1975 *Sov. Phys.–JETP* **40** 1158
[32] Endo T and Kino T 1979 *J. Phys. Soc. Japan* **46** 1515
[33] Kogure Y and Hiki Y 1975 *J. Phys. Soc. Japan* **39** 698
[34] Kus F W and Taylor D W 1982 *J. Phys. F: Met. Phys.* **12** 837
[35] Serebrjany E M 1991 *J. Phys. A: Math. Gen.* **24** 4067